Space Weather

RESEARCH ARTICLE
10.1029/2025SW004857

How Does the Definition of a Geomagnetic Storm Affect the Contents of the Resulting Storm List?

Atlas M. Patrick[1], John C. Coxon[1], Sarah N. Bentley[1], Maria-Theresia Walach[2], Kyle R. Murphy[1], I. Jonathan Rae[1], and Isobel S. Lockley[3]

[1]School of Engineering, Physics and Mathematics, Northumbria University, Newcastle upon Tyne, UK, [2]Lancaster University, Lancaster, UK, [3]Department of Physics, University of Warwick, Coventry, UK

Abstract A geomagnetic storm is a significant and prolonged disturbance of the Earth's magnetic field caused by an enhancement of the ring current. Storms are typically identified using magnetic field measurements from multiple ground-based magnetometers, and the corresponding dates and times of multiple storms can be collated to form a storm list. There is currently no quantitative definition of a geomagnetic storm, so the contents of a particular storm list are highly dependent on the identification criteria that were used to generate it. The different definitions and identification methods can cause the physical properties of storms in different lists to vary, and these variations may be significant. We take several storm lists with different identification methods, and we compare the probability distributions of a range of solar wind variables and geomagnetic indices between those lists. We also compare the temporal behavior of the storm lists, and discuss how the differences may affect the way geomagnetic storms are defined and studied. We find that changing the definition of the quiet time has a direct impact on the start and end times of the storms, and this can result in a storm being significantly shorter when defined using a more negative quiet time definition. We also find that changes to the threshold value of minimum magnetic disturbance have a greater impact on the properties of the identified storms than changes to the quiet time definition. We provide recommendations on which storm lists to use for different scenarios.

Plain Language Summary A geomagnetic storm is a period of time when the Earth's magnetic field changes significantly from its usual behavior. This change is caused by particles from the Sun entering the Earth's magnetic field, increasing the amount of charged particles that are orbiting the Earth, and this results in a change in the strength of the ring current. The change creates a magnetic field, which affects magnetic field measurements that are made on Earth. There isn't yet a specific definition of what exactly a geomagnetic storm is, as the criteria can vary between sources. This means that when a large number of storms are found and a list of the times that they occurred is created, the contents of the list are highly dependent on how geomagnetic storms were defined. The differences in the definitions may cause the physical properties of the storms in the resulting lists to be different, and this could affect the science that is done using the storm lists.

Key Points:

- The definition of a storm can greatly affect the properties of the list, with the threshold value and quiet time having significant impacts
- Properties of the pre and post-epoch phases of storms are physically distinct, and the behavior is not greatly affected by storm definition
- We recommend using the Walach and Grocott (2019, https://doi.org/10.1029/2019JA026816) storm list for most applications

Supporting Information:

Supporting Information may be found in the online version of this article.

Correspondence to:

A. M. Patrick,
atlas.patrick@northumbria.ac.uk

Citation:

Patrick, A. M., Coxon, J. C., Bentley, S. N., Walach, M.-T., Murphy, K. R., Rae, I. J., & Lockley, I. S. (2026). How does the definition of a geomagnetic storm affect the contents of the resulting storm list? *Space Weather*, *24*, e2025SW004857. https://doi.org/10.1029/2025SW004857

Received 26 NOV 2025
Accepted 4 MAY 2026

Author Contributions:

Conceptualization: John C. Coxon, Sarah N. Bentley
Data curation: Maria-Theresia Walach
Formal analysis: Atlas M. Patrick, Isobel S. Lockley
Investigation: Atlas M. Patrick
Methodology: Atlas M. Patrick
Resources: Maria-Theresia Walach, Kyle R. Murphy
Supervision: John C. Coxon, I. Jonathan Rae
Visualization: Atlas M. Patrick
Writing – original draft: Atlas M. Patrick

1. Introduction

The solar wind is the plasma that flows outward from the Sun and is made up of highly energized ions and electrons which originate in the solar corona. As it flows outwards through the solar system, it drags the sun's magnetic field with it, which is known as the interplanetary magnetic field (IMF). The conditions of the solar wind and the IMF at Earth are highly variable, both due to the changeable behavior of the Sun as well as the Earth's relative position in the Solar System. When the IMF is directed southwards, in the opposite direction to the Earth's magnetic field, the IMF field lines can interact with the field lines of the Earth's magnetic field in a process called magnetic reconnection (Dungey, 1961; Fu & Sun, 2026; Sonnerup et al., 1981). The open magnetic field lines that are formed during reconnection allow plasma to cross the magnetopause boundary and enter the magnetosphere, and the process continues until the IMF is no longer southward pointing (Cowley & Lockwood, 1992; Eggington et al., 2022; Siscoe & Huang, 1985; Trattner et al., 2007, 2017).

Magnetic reconnection at Earth is commonly described using the Dungey cycle, where the southward pointing IMF reconnects to the northward geomagnetic field, and the resulting open magnetic field lines are dragged antisunward across the poles by the solar wind (Dungey, 1961; Fu & Sun, 2026). This is a simple description that is able to explain many characteristics of the Earth's magnetosphere, however the original model assumed steady and equal rates of dayside and nightside reconnection. We now know that magnetospheric dynamics are much

Writing – review & editing: Atlas M. Patrick, John C. Coxon, Sarah N. Bentley, Maria-Theresia Walach, Kyle R. Murphy, I. Jonathan Rae, Isobel S. Lockley

more complex than in the Dungey model, which has lead to improved reconnection models such as the Expanding/Contracting Polar Cap model (Siscoe & Huang, 1985; Walach et al., 2017) and Dual-Lobe reconnection (Cowley, 1981; Milan et al., 2020).

Charged particles originating in the solar wind and ionosphere are accelerated and transported by a variety of mechanism in the current sheet, to contribute to the ring current. Both sources of particles are enhanced during intense periods of magnetospheric activity, which can be caused by coronal mass ejections (CMEs) and stream interaction regions (SIRs) (Gonzalez et al., 1999; Hutchinson et al., 2011; Kataoka & Miyoshi, 2006; Samwel & Miteva, 2023). These events allow for large amounts of solar wind plasma enter the magnetosphere. This plasma moves into the inner magnetosphere from the magnetotail plasma sheet (Cramer et al., 2017), where it can affect the radiation belts, enter the upper atmosphere, and enter the ring current (Forsyth et al., 2014; Sandhu et al., 2018, 2021). Times of enhanced convection also allow for particles from the ionosphere to enter the magnetotail plasma sheet and be transported to the ring current similarly to the movement of solar wind particles (Daglis, 2006). Positively charged ions with energies in the range of ∼10 to ∼100 keV (Daglis et al., 1999) that enter the ring current will contribute to the total current density, and increase the ring current strength.

The ring current flows westwards around the Earth near the equator and is caused by curvature drift. This drift causes the particles to drift transversely to the magnetic field lines, and as positive and negatively charged particles drift in opposite directions there is a separation of charges, which causes the ring current (Daglis et al., 1999). The charged particles from the solar wind and ionosphere can enter the ring current, and a net gain in ring current plasma will cause the ring current strength to increase (Kivelson & Russell, 1995; Williams, 1985). Once the amount of magnetic reconnection with the solar wind decreases, the charged particles in the ring current can charge exchange with neutrals, which causes them to no longer undergo curvature drift as they become uncharged, and they can escape the magnetosphere. The ions that are created as a result of these charge exchange processes typically have low energies, reducing the total energy in the ring current (Dessler & Parker, 1959; Daglis et al., 1999, references therein).

When the ring current's strength increases it induces a reduction in the measured magnetic field strength at the Earth's surface, and a significant reduction can be classified as a geomagnetic storm (Akasofu & Chapman, 1961; Gonzalez et al., 1994). This magnetic disturbance can be measured using several ground-based magnetometers, and the data can be used to create a storm index. The indices that are commonly used in the study of geomagnetic storms are Disturbance Storm Time (Dst) and SYM-H, which have some differences in how they are determined but are roughly equal in magnitude at intensities of around −30 to −300 nT (Hutchinson et al., 2011; Wanliss & Showalter, 2006). There are other indices that can be used to study geomagnetic storms, such as the Kp and aa indices, however in this paper we focus on SYM-H and Dst as they are the most similar and are commonly used.

Disturbance Storm Time (Dst) is measured using four magnetometer stations. These stations are roughly evenly spaced around the Earth, in Hermanus, Kakioka, Honolulu, and San Juan, which were chosen as they are located at a sufficient distance from the auroral and equatorial electrojets to avoid detecting magnetic perturbations associated with them (Sugiura & Kamei, 1991). Dst has a time resolution of 1 hr and relies on an assumption that the ring current system is symmetrical, which is no longer fully accepted (Bergin et al., 2020; Campbell, 2004).

SYM-H is a measure of the symmetrical part of the horizontal component of the terrestrial magnetic field near the equator (Wanliss & Showalter, 2006). SYM-H is determined by averaging the measured disturbance at each of six magnetometer stations, with a latitudinal correction, and has a time resolution of 1 min, significantly higher than Dst. SYM-H is found using a set of 10 stations that can be used interchangeably to obtain 6 measurements, using the assumption that the ring current is parallel to the equatorial plane of the Earth's magnetic dipole (Iyemori, 1990).

Ring current indices can be used as an imperfect proxy for the ring current energy, where a decrease in the index implies an increase in the amount of energy stored in the ring current (Sandhu et al., 2021). This can allow for the ring current to be studied without the need for a large number of in situ spacecraft, although there is a significant amount of contamination from other current systems.

The two storm indices are sometimes used interchangeably (e.g., Murphy et al., 2018; Ohtani et al., 2001), despite their differences, and this may bias the results that are found. The calculation of SYM-H involves mid-latitude magnetometer stations, which may cause the measurements to be influenced by local current systems that would not affect Dst measurements. There is also a systematic difference between Dst and SYM-H which has

been found to increase at the peak of geomagnetic storms, and the size of the error correlates with the strength of the storm, which is caused by the way the measurements from the magnetometer stations are compiled into a single magnetic perturbation value (Katus & Liemohn, 2013).

Geomagnetic storms are commonly defined using the magnitude of the maximum negative magnetic disturbance as measured on Earth, typically using SYM-H or Dst. Based on the behavior of the magnetic field, they are typically split into three phases: the initial, main, and recovery phases (Echer et al., 2011; Gonzalez et al., 1999; Hutchinson et al., 2011; Tsurutani et al., 2006; Walach & Grocott, 2019).

The initial phase is the first phase of the storm, but it is also the least well-defined. The initial phase can be defined as starting when the solar wind dynamic pressure increases and compresses the magnetopause closer to the Earth (Gonzalez et al., 1999; Murphy et al., 2018; Shue et al., 1998; Staples et al., 2022), and can also be identified using measurements of the Earth's magnetic field (Joselyn & Tsurutani, 1990; Perreault & Akasofu, 1978; Walach & Grocott, 2019). The exact point at which the initial phase begins is not yet widely agreed upon (Collado-Villaverde et al., 2024; Yokoyama & Kamide, 1997). One definition that uses magnetic field measurements is that the initial phase begins at the time of maximum positive disturbance before the sudden reduction in the magnetic field strength (Hutchinson et al., 2011), but it can also be defined as the point where the magnetic field is at the quiet level, before it reaches a maximum positive disturbance (Walach & Grocott, 2019).

The main phase is the period in which the most extreme behavior occurs, and it ends at the time of maximum negative magnetic disturbance. The main phase is typically a period of strong southward IMF ($B_z \leq -5$ nT) (Gonzalez et al., 1994; Kumar et al., 2026) which drives rapid magnetic reconnection, allowing energetic particles in the solar wind plasma enter the magnetosphere, enhancing the ring current strength and causing the decrease in the surface magnetic field that characterizes geomagnetic storms (Parker, 1962).

The recovery phase is the final phase, where the changes to the magnetosphere that occurred during the storm gradually return to the ambient level. The recovery starts at the time of maximum magnetic disturbance, which is the time that is typically identified in storm lists, and ends when conditions return to quiescence. The definition of the ambient level of Dst or SYM-H can vary slightly from list to list, however, irrespective of the exact definition, the recovery phase is the longest of the three phases, sometimes lasting for several days (Walach & Grocott, 2019).

Many studies have compiled lists of storms in order to study the phenomenon statistically (e.g., Echer et al., 2011; Kataoka & Miyoshi, 2006; Murphy et al., 2018; Thomas et al., 2016; Turner et al., 2015; Walach & Grocott, 2019). While the details of each list's definition of a geomagnetic storm will vary, the vast majority use look for the maximum negative disturbance in SYM-H or Dst to be below a threshold value. This threshold value is typically set to −50 nT (Gonzalez et al., 1994, 1999), but other values have been used (Kataoka & Miyoshi, 2006; Walach & Grocott, 2019). In this paper we investigate the quantitative definitions of geomagnetic storms that are used when creating storm lists, and we use the term “storm definition” to refer to the numerical criteria that are used to generate storm lists.

The time of maximum disturbance is the end of the main phase of the storm, and is commonly referred to as the epoch time. Some lists also identify the start and end of the storms as well as the epoch (Murphy et al., 2018), and the start and the end of the initial and main phases may also be included in the storm list (Hutchinson et al., 2011; Walach & Grocott, 2019). Some storm lists may be created by identifying the storms by eye, either wholly or in part (Hutchinson et al., 2011), which may not involve a strict set of criteria and has ramifications for reproducibility. The resulting lists are a set of timestamps that correspond to the identified storm times, and they are used widely in literature (e.g., Bower et al., 2025; Coxon et al., 2023; Killey et al., 2025; Sandhu et al., 2021), which means that a single list can be the basis of a large amount of research, and the way the initial list was created could have far-reaching repercussions.

In this paper, we will first discuss the main physics concepts involved with the understanding and the study of geomagnetic storms, including solar-terrestrial interactions and the structure and behavior of the Earth's magnetosphere. We will then go into further detail on the properties and typical behaviors of geomagnetic storms, and the most common ways that storm lists are created. We will outline the main storm lists that were used in this investigation in Section 2, and explain briefly how the storms in each list were identified. We will then detail the methods and techniques that were implemented in order to compare the lists in Sections 3 and 4, and discuss the

Table 1
Details of the Storm Lists That We Use in This Investigation, Alongside the Shortened Labels That We Use in This Paper

Original paper	Our label	Index	Threshold value (nT)	Time period covered	Number of storms
Kataoka and Miyoshi (2006)	KM06	Dst	−100	1996–2004	55
Echer et al. (2011)	E11	Dst	−50	1957–2008	933
Turner et al. (2015)	Tu15	SYM-H	−50	2012–2015	51
Thomas et al. (2016)	Th16	SYM-H	−50	2001–2013	139
Murphy et al. (2018)	M18	SYM-H and Dst	−50	1996–2022	443
Gabrielse et al. (2019)	G19	SYM-H	−50	2008–2016	161
Walach and Grocott (2019)	WG19	SYM-H	−80	1981–2024	538
Hua et al. (2022)	H22	SYM-H	−50	2013–2018	118

implications of the results in Section 5. Finally we present our conclusions in Section 6, and give suggestions on how to select a storm list for future research in Section 7.

2. Data

In this investigation we use both SYM-H from the OMNI data set and Dst data from Kyoto WDC for 1981 to 2024. Although both SYM-H and Dst measure the disturbance in the Earth's magnetic field caused by changes to the ring current, the data and methods used to derive them have differences that may affect how geomagnetic storms are identified when using one index over another, which is why we use both indices.

2.1. Storm Lists

Here we introduce the lists we use by order of publication, and a concise list of the main properties of the lists is given in Table 1. In this paper we only consider lists that identify storms using SYM-H or Dst thresholds. There are also identification methods that use a minimum rate of change of SYM-H or Dst (e.g. Balan et al., 2017; Partamies et al., 2013), and we may investigate these in a future paper. We acknowledge that these storm lists were created for specific purposes and were not made to be compared in this way. The aim of this investigation is not to criticize any of the storm lists we compare, but to simply highlight the differences between them and make readers aware of the potential consequences of using storm lists outside of their designed context without ensuring the lists are suited to the purpose.

KM06 is made up of Lists A, B, and C from Kataoka and Miyoshi (2006), which originally separated the storms into different lists based on whether they were driven by CMEs or SIRs. For this investigation we combine the three lists to obtain a single, longer list. For the storms associated with CMEs and SIRs, the arrival time of the shock/stream interface is given, and the time separation between the shock/interface and minimum Dst was used to define the time of the storm, with a threshold value of −100 nT imposed on the minimum Dst value. Due to the relative cadences of Dst and SYM-H that were previously mentioned, the time of minimum Dst can only be given to the nearest hour, so caution is required when comparing this list to lists that were derived from SYM-H data.

This is also the case for the next list, E11 (Echer et al., 2011), which covers the longest timespan of all the lists we considered, from 1957 to 2008, however, to be able to use SYM-H data to analyze the storms in this list we removed the storms that occurred before 1981. This allows for the behavior of geomagnetic storms to be investigated over many solar cycles. The storm epoch times were determined using a Dst threshold of −50 nT.

Tu15 (Turner et al., 2015) covers only a time range of 2012–2015. This short time period means that the list will not be useful when studying the occurrence of geomagnetic storms over time, however the properties of the storms themselves can be compared to the other lists. The storms were found using a SYM-H threshold value of −50 nT to identify the epoch, which was then confirmed by eye. Storms with overlapping main phases were removed, and the epoch time of storms with complex signatures were taken to be the lowest SYM-H value.

Th16 (Thomas et al., 2016) was generated using data from Kyoto WDC, from which the time of main phase onset and the time of minimum SYM-H were determined. Some of the times were then manually adjusted, using a SYM-H threshold of −50 nT, however, the details of these adjustments or the way in which the time of main

phase onset was defined is not clear. Storms with minimum SYM-H of less than −200 nT were also removed from the list.

M18 (Murphy et al., 2018) originally consisted of storms from 2012 to 2016 using a SYM-H threshold of −50 nT, and was then expanded to cover a time period from 1996 to 2022. The expanded list did not use a pre-defined SYM-H or Dst threshold to identify the storms, and instead found the storms based on the overall behavior of the magnetic field measurements, and used solar wind data to identify the start and end of the storms. In both lists the epoch time was defined as the time of minimum Dst, and all the times are given with hourly resolution. In this investigation we use the expanded list, but we use the original list's threshold value by removing all of the storms that do not cross −50 nT. We also use the original, un-thresholded list where there are differences between the two, and in these cases we refer to the original list as M18*.

G19 (Gabrielse et al., 2019) uses a SYM-H threshold of −50 nT to define a geomagnetic storm, and sets the epoch time as the time of lowest SYM-H within 24 hr of crossing the threshold value. The time of most positive SYM-H in the 24 hr prior to the epoch is defined as the main phase onset, and the end of the recovery phase is defined as the time when SYM-H recovers to 80% of the minimum. G19 covers a time period from 2008 to 2016, and also gives the driver of each of the storms—CME, HSS (high-speed stream), both, or other.

WG19 (Walach & Grocott, 2019) uses SYM-H data, a storm threshold of −80 nT and a quiet time definition of 15 nT to identify the start and end time of each of the three storm phases, using an algorithm similar to that used by Hutchinson et al. (2011). We also considered the lists created by Wharton et al. (2020) and Sandhu et al. (2021), however, they use the same algorithm as the WG19 list, so we do not examine these lists explicitly. Additionally, we create a derived storm list using the same algorithm, but we change the threshold to −50 nT; we call this list WG19-50 in the text. WG19 is the only list in our selection which specifically identifies the start and end of all three phases of each storm.

H22 (Hua et al., 2022) identifies storms using a SYM-H threshold of −50 nT, with the lowest value used when multiple events occurred within 2 days of each other. The original investigation focussed on electron fluxes from 2 days before the epoch time to 4 days after, so we took these times to be the start and end of the storms as the list only specifies the time of minimum SYM-H.

For the storm lists that do not specify a start or end time for the storms, we impose set lengths for the recovery phase, and the initial and main phase combined. We use methodology based on Thomas et al. (2016) and set the pre-epoch length to one and a half days and the post-epoch length to 3 days. This is applied to the storms in KM06, E11, and Tu15. The pre-epoch length of the storms in G19 and Th16 are set to one day + the length of the main phase, due to the start of the main phase being specified in the lists. We acknowledge that this will affect the properties of the resulting geomagnetic storms in these lists, but it is necessary to be able to compare the storm lists to one another.

In Figure 1, a single geomagnetic storm event is shown, with the colored bars indicating how the storm would be identified by each storm list. The yellow, red, and green sections indicate the initial, main, and recovery phase, respectively, or the pre-epoch and post-epoch phases for storm lists which do not identify the phase times. From this we can see that the different geomagnetic storm identification methods and their subsequent storm lists result in very different subsets of the same storm. This means that any subsequent work will therefore be biased to certain parts of each storm, depending on the storm list used.

In addition to the storm lists previously mentioned, we also considered lists created by Loewe and Prölss (1997), Yokoyama and Kamide (1997), Zhang et al. (2006), Reeves et al. (2003), Yermolaev et al. (2010), Hutchinson et al. (2011), and Manu et al. (2023), but we were ultimately unable to include these in our investigation due to the lists not being easily accessible.

3. SYM-H Distribution of Different Lists

We compare the contents of each storm list, that is, the physical properties of the storms that each list identifies. We take all of the SYM-H data between the start and end time for each storm in each list to be the contents of the list, or from one and a half days before the epoch to 3 days after the epoch for the lists that do not give start and end times. We use a bootstrapping algorithm to verify that the resulting probability density functions were due to an underlying physical property of the storms within the lists and not simply due to the small sample size.

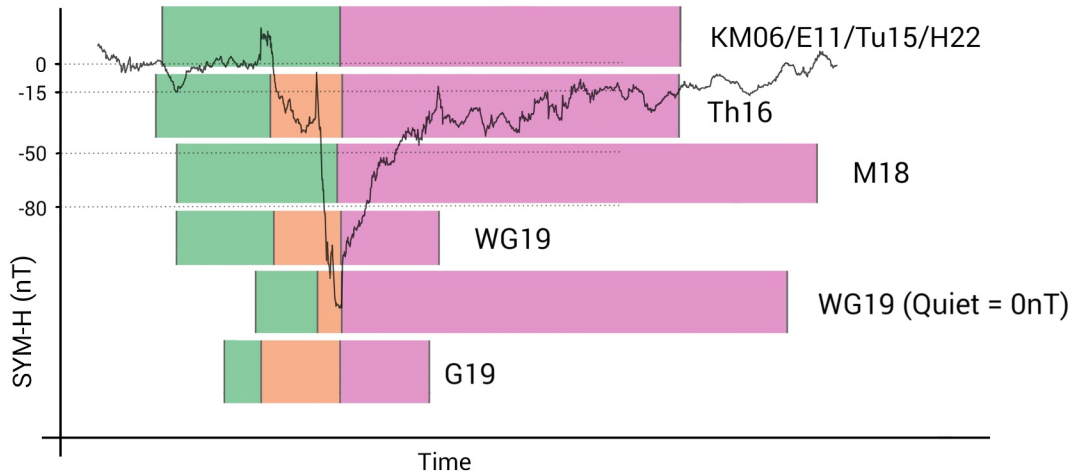

Figure 1. Diagram showing how the geomagnetic storm that occurred on 01/10/2012 would be identified differently by the methods used to generate the various storm lists. The green, orange, and pink sections indicate the initial, main, and recovery phase, respectively, or the pre-epoch and post-epoch phases for storm lists which do not identify the phase times.

Bootstrapping is a method of resampling a data set to create a large number of subsamples, which reduces the amount of uncertainty in the results. Using the technique employed by Love et al. (2015), we choose our subsamples to be the same length as the original storm list and to be made up of storms chosen randomly with replacement. The total number of subsamples we generate is determined using the formula $N \sim n(\log n)^2$ (Babu & Singh, 1983), where N is the total number of subsamples, and n is the size of the original data set, which in this case is the number of geomagnetic storms in a particular storm list.

After we obtain our larger data sets we find the mean distribution and standard deviation of the probability density distribution of each subsample. To verify that the shape of the probability density function is indicative of the true distribution and not influenced by the size of the histogram bins, we use a Kernel Density Estimation method of plotting the distribution curve and comparing the shape of the curves with the histograms. This comparison can be found in Supporting Information S1. We find no significant difference between the two distributions so use histograms for our analysis going forwards.

3.1. Storm Times

Figure 2 shows the distribution of storm time SYM-H values for all the storm lists compared with the distribution of all the SYM-H values between the start of the first storm and the end of the last storm in the list, which we refer to as the background. From Figure 2, we can see that the distribution of SYM-H values for all the storm lists favor more negative values than the background, as expected. The M18, Th16, Tu15, E11, and KM06 distributions all have the same overall shape, with a single peak at around −20 nT with the distribution decaying more slowly on the negative side than the positive side. The KM06 distribution is the flattest, and the M18 distribution is the most similar to the background distribution. We do not see the single peaked structure in the two WG19 distributions; in Figure 2a there is a clear dip in the SYM-H distribution at −15 nT, which is also seen in Figure 2b. From this we can infer that the probability density function of the WG19 lists is a superposition of multiple different probability density functions.

We test our inference by splitting the WG19 distribution by the times identified to be the start and end of the three storm phases and plot Figure 3 which shows the initial, main and recovery phase distributions which have very different structures. The initial phase has a narrow peak at around 10 to 0 nT, and the main and recovery phases have wide distributions that do not go above the quiet level. In Figure 3d, we can see that the double-peaked structure seen in Figure 2 is due to the superposition of the three phase distributions. On the left side are the distributions for the original WG19 list that uses a quiet time definition of 15 nT, and on the right side is the distribution of the WG19-0 list which was generated using the same algorithm as the original list, but uses a quiet time definition of 0 nT. We can see that the position of the trough corresponds directly to the definition of quiet time that was used to generate the list.

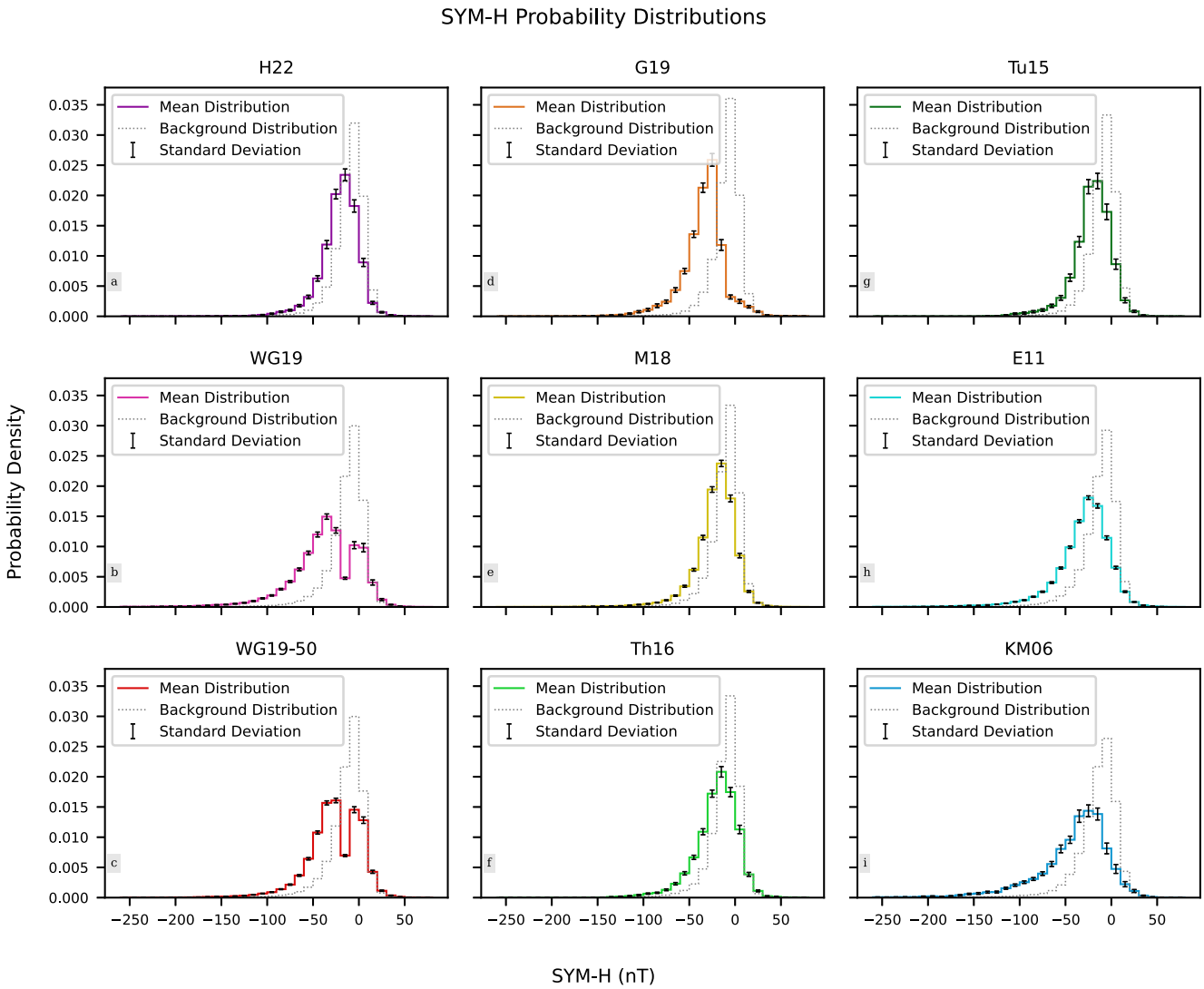

Figure 2. Difference between the storm time SYM-H distributions for each storm list. The colored distributions show the mean distribution, and the standard deviation of the bootstrapped subsamples is shown by the error bars. The dotted line shows the distribution of all the SYM-H data for the time between the start of the first storm and the end of the last storm in the list, which is called the background distribution.

To test if this effect is seen in the other lists, we split the all storms into pre- and post-epoch phases and plot Figure 4. We can see that the pre-epoch distribution favors higher values of SYM-H than the post-epoch distribution, and that the overall distributions for all the lists are also superpositions of multiple distributions, but they are not as distinct as the WG19 distributions.

The Wasserstein distance (Kantorovich, 1960; Vaserstein, 1969) is defined as the area between two Empirical Cumulative Distribution Functions (ECDFs), and a larger Wasserstein distance indicates a greater difference between the distributions. We compute ECDF of each storm list, which is given in Supporting Information S1, and find the Wasserstein distance for each pair of lists. The results are given in the form of a heatmap as shown in Figure 5.

From Figure 5, we find that G19 and E11, and H22 and M18 are the most similar to one another, and that Tu15 and KM06, and H22 and KM06 are the most different. We also see that KM06 is consistently different to the other lists, and that WG19 is more different to every list than WG19-50, except for KM06. WG19-0 was generated using the same algorithm as the original WG19 list, with the definition of the quiet time changed to 0 nT from −15 nT. By comparing the WG19, WG19-0, and WG19-50 Wasserstein distances, we can see that the change of threshold value has a much larger effect on the SYM-H distribution in the resulting storm list than a change in

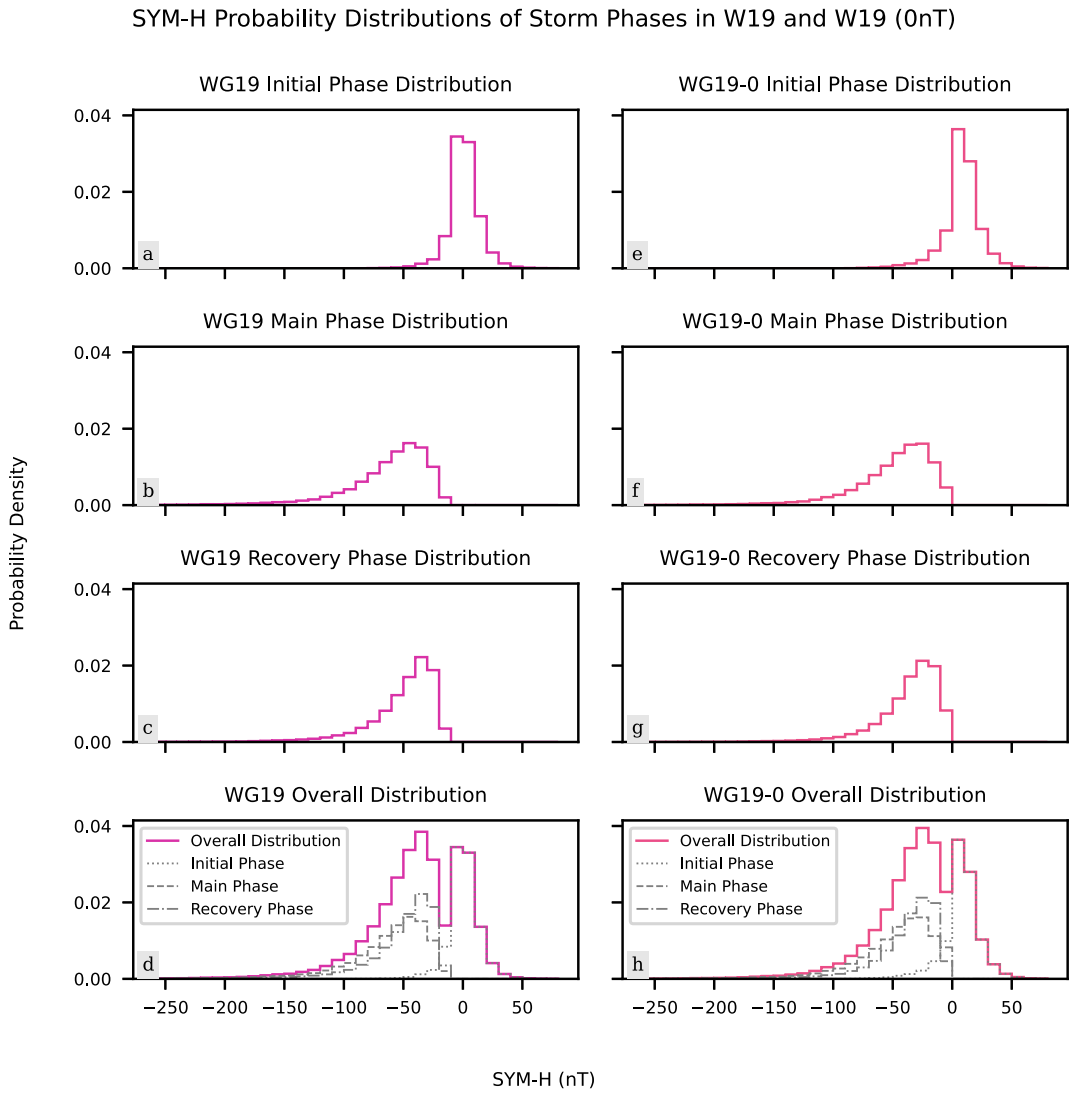

Figure 3. Probability Distributions of the three storm phases identified by WG19, using a quiet time threshold of −15 nT in the left column and 0 nT in the right column. The top row shows the probability density of the initial phase of the storms, the second row shows the distribution of the main phase, the third row shows the distribution of the recovery phase, and the fourth row shows the sum of the distributions of the three phases, given by the solid colored line, and the three phase distributions as the dotted and dashed lines.

quiet time definition. The full set of Wasserstein distances we computed can be found in Supporting Information S1.

3.2. Quiet Times

Although storm lists provide time stamps that relate to the time of geomagnetic storm occurrence, they can also be used to investigate non-storm time, or quiet time, by simply removing the times that they define as being in a geomagnetic storm from the data set. Due to the way some storm lists deal with complex or extreme storms, this could result in very different quiet time distributions. For example, Th16 removes any storms with SYM-H minima below −200 nT, which would result in these extreme storms being defined as "quiet time" in our methodology.

We determine the probability distribution of the quiet time as defined by each of the storm lists, for the time between the end of the first storm in the list and the start of the final storm. This allows us to compare not only the

10.1029/2025SW004857

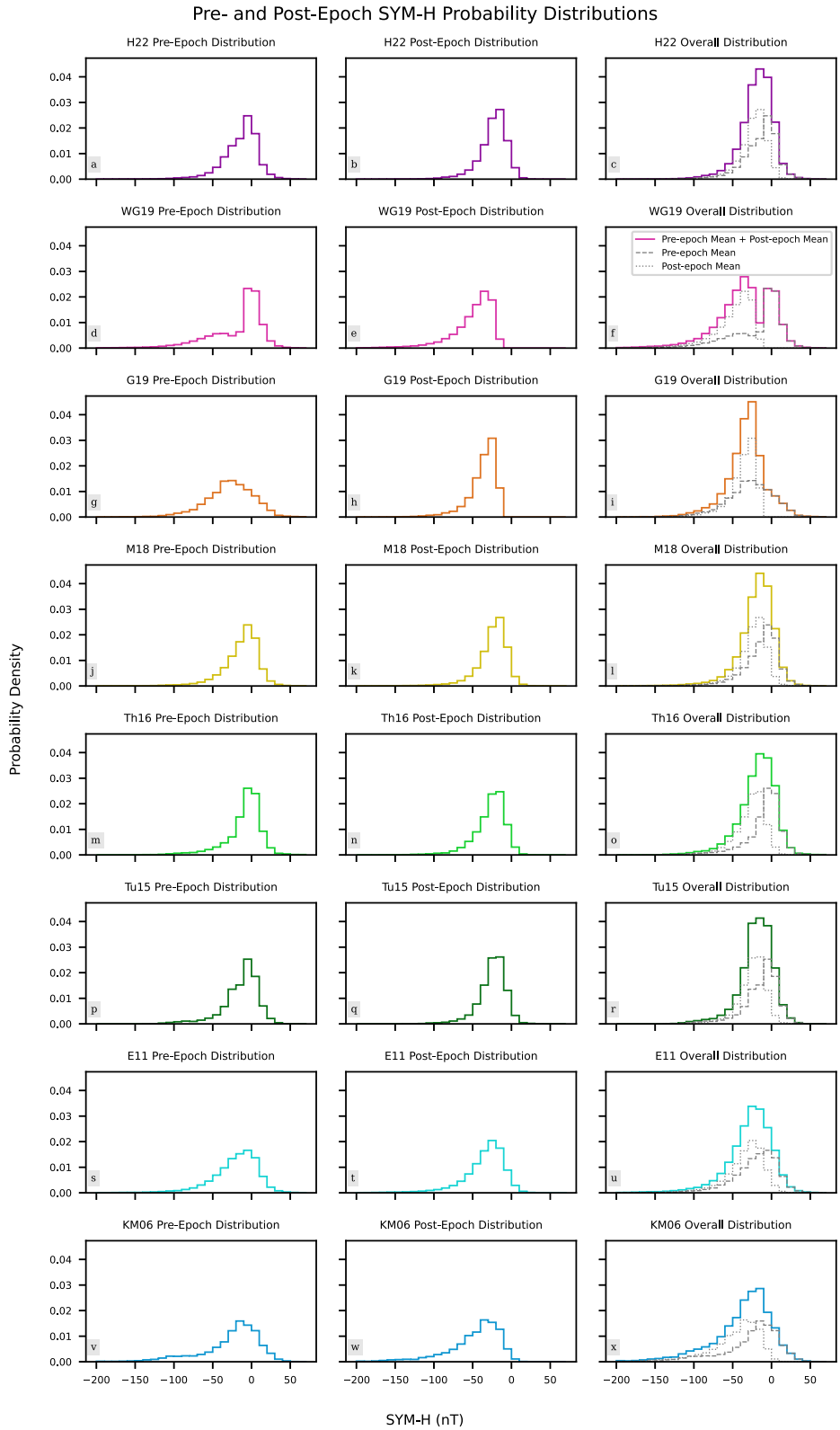

Figure 4. Pre- and post-epoch SYM-H probability distributions for each storm list. The columns are (from left to right): pre-epoch distribution, post-epoch distribution, overall distribution of the entire storm. Each row has a separate storm list, and all the plots are given on the same axes and so can be directly compared.

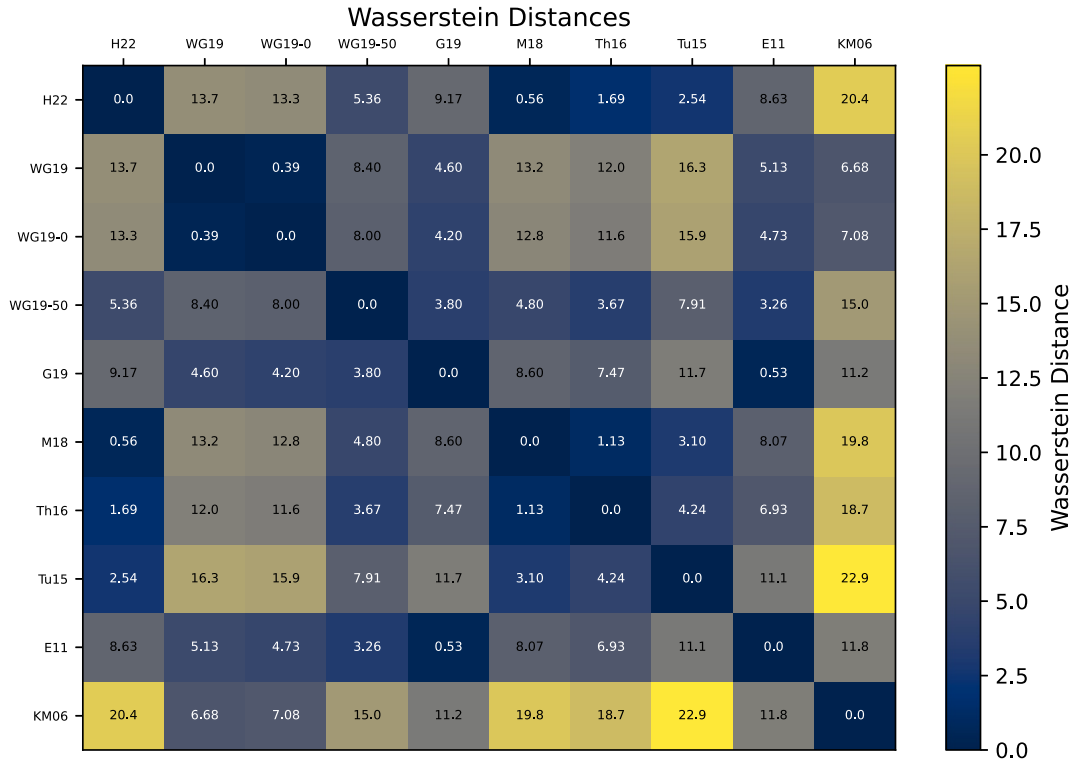

Figure 5. Heatmap of the Wasserstein distances between each pair of storm lists. The larger the Wasserstein distance the brighter the color, and the more different the lists are.

possible effects of selecting a particular storm list for an investigation due to the properties of the storms but also what the identification method may have missed.

We find the probability density functions of the quiet times for each list in the same way as we do for the storm times. Figure 6 shows the probability density distribution of all non-storm times for each storm list, plotted alongside the background distribution. The distributions of all the lists show the same general single-peaked shape, where the quiet time distribution is lower than the background for more negative SYM-H values, and becomes higher than the background at larger values of SYM-H. This trend is not as clear in the KM06 distribution, as the quiet and background distributions are almost identical, likely due to the more negative threshold value and the shorter storm list created as a result. We can also see that the Th16 distribution is similar to the distributions of the other lists, which implies that the exclusion of storms with SYM-H minima less than −200 nT does not have a large effect on the quiet time distribution. This is to be expected, as (Thomas et al., 2016) only found eight storms with minima less than −200 nT in the time period that their list covered.

4. Temporal Properties of Storms

We use a superposed epoch analysis (SEA) where the time of minimum SYM-H is set as the epoch. Each of the storms in a particular list is overlaid with the others, centered on the epoch, which allows for the median behavior of the storms in a certain list to be found, as well as the interquartile range.

Figure 7 shows the median and interquartile range of the SYM-H of the storms in the relevant list. For ease of understanding, the data is cropped to a time period between one day before the epoch and 3 days after the epoch, as this is the period covered by all of the storms in all of the lists, and it also allows for the temporal behaviors to be seen clearly.

In Figure 7, we can see that the storms in all the lists have the same overall behavior in the time period that we have focused on. The depth of the dip at the epoch and the steepness of the recovery is directly connected to the threshold value required to identify a storm, which can be seen by the fact that KM06 has the steepest gradients due to having the most negative threshold value of −100 nT, whereas the storm lists which used a threshold of

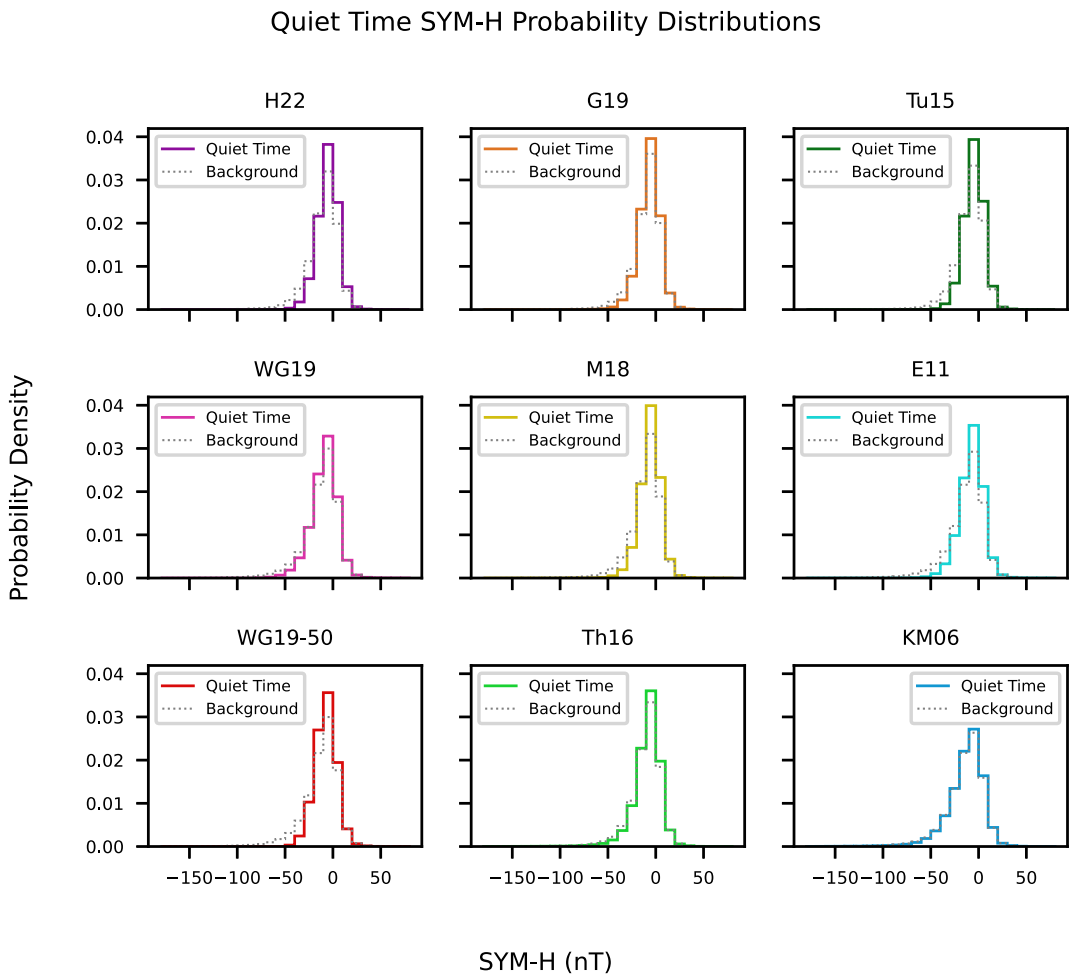

Figure 6. Quiet time probability distribution functions for each of the storm lists, where the colored lines are the mean distribution of quiet time SYM-H and the dotted line indicates the background distribution.

−50 nT have a shallower gradient. In both WG19 plots we can see that the lower quartile has a slight "elbow" at around −0.75 days which is not present in the other plots, and this is very likely due to the fact that 21 of the storms have pre-epoch times of less than one day, which results in a widening of the lower quartile due to the loss of data. This shows that the specific definitions of the storm phases that were used to create WG19 can result in noticeable differences with storm lists that do not specify the start and end of storms.

We then calculate the median temporal behaviors of each subsample and find the median and interquartile range of these medians. The result of this is compared with Figure 7. Both methods result in almost identical plots, implying that our results are free from selection effects.

Figure 8 shows the SEA of E11 and KM06 using Dst data, as this is what was used to generate the storm list. It is clear that the overall shape of the storm trace is very similar to those plotted using SYM-H data, however the hourly resolution of Dst results in a lower level of detail. We also see that in Figure 7 the upper quartile of both E11 and KM06 reaches values greater than zero, however in Figure 8 the maximum value of the upper quartile in both lists does not cross zero. This discrepancy between the Dst and SYM-H data is small and understood (Bergin et al., 2023; Katus & Liemohn, 2013; Sandhu et al., 2021), but could still pose issues if Dst and SYM-H are assumed to be interchangeable.

4.1. Storm List Overlaps

We find the percentage overlap between storm lists by determining if, for each storm in List A, there is a storm that occurs at the same time in List B. We defined "storms that occur at the same time" as storms with their epochs

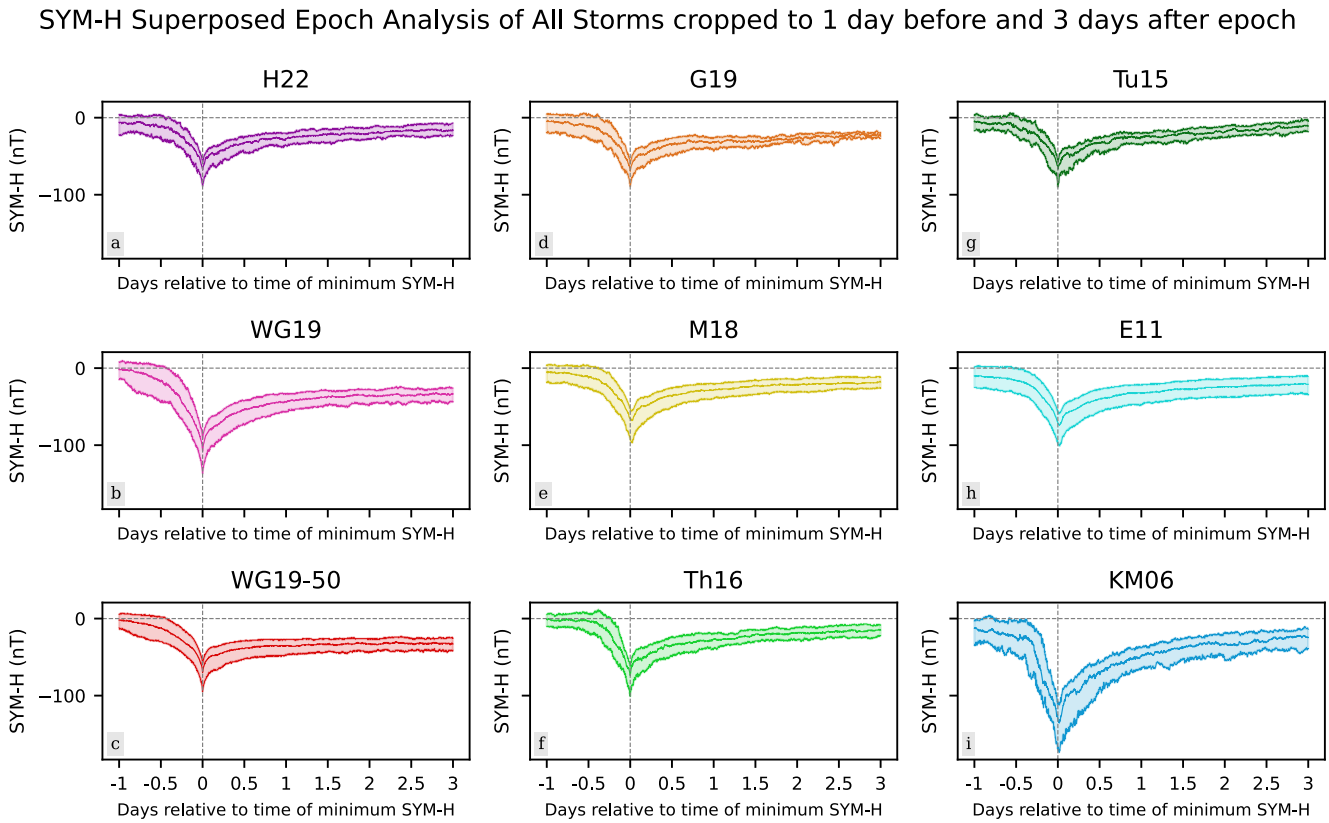

Figure 7. Superposed epoch analyses of each of the storm lists, with the median shown as a solid line and the interquartile range as the shaded region. The storms have been cropped to a period of one day before the epoch and 3 days after the epoch to make the behaviors and differences between the lists more visible. Only the original WG19 list with a quiet level of −15 nT has been included in this plot because the overall shape of the different WG2019 storms does not differ significantly between lists. The superposed epoch analysis of the individual WG19 lists can be found in the Supporting Information S1.

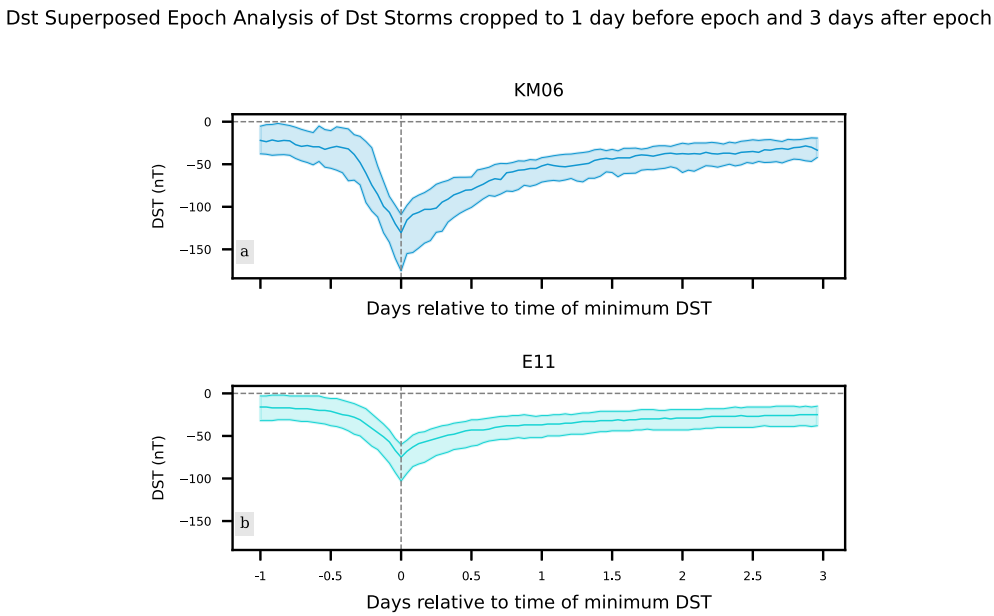

Figure 8. Superposed epoch analyses of KM06 and E11, generated using Dst data. The storms have been cropped to a period of 1 day before the epoch and 3 days after the epoch.

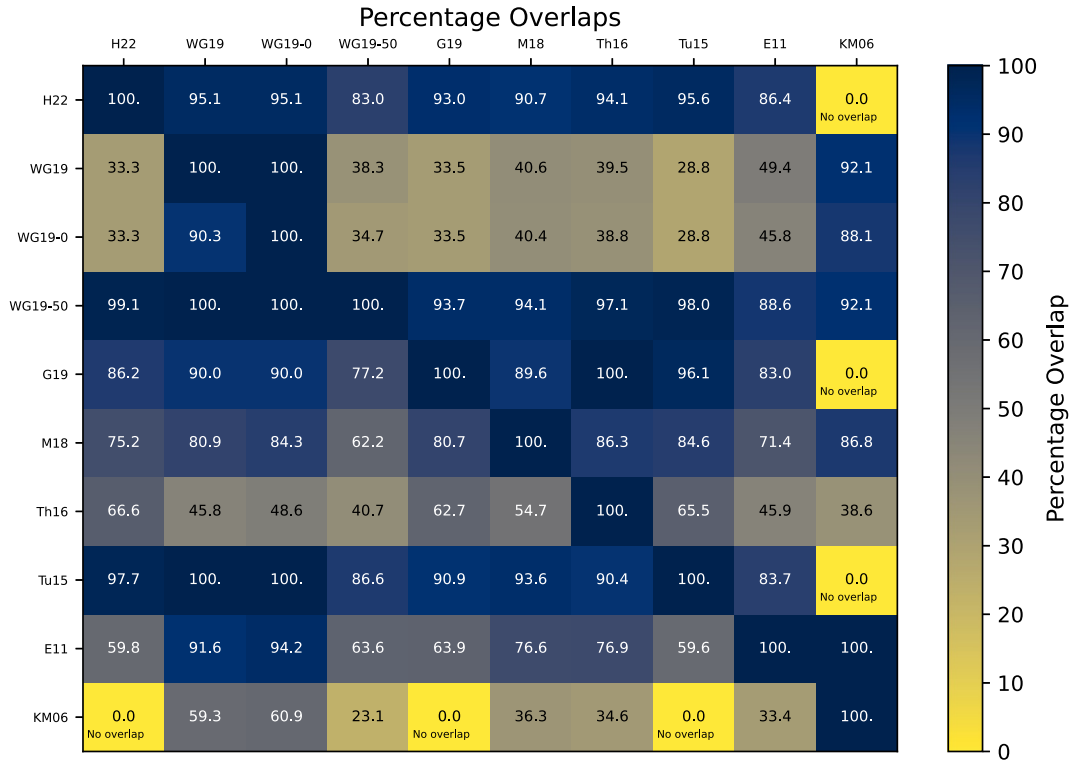

Figure 9. The percentage of storms in the list on the *x*-axis that are also in the list on the *y*-axis, for the time period over which both storm lists overlap. Storms are defined as being in both lists if there is a storm in List A that has its epoch within 12 hr of a storm in List B. The brighter the color the more different the storm lists are.

within 12 hr of one another to account for any slight discrepancies caused by identification methods. The percentage overlaps are shown in Figure 9. We also only compare lists in the time period over which they overlap, and the number of days each pair of storm lists overlap is given in Supporting Information S1.

From Figure 9 it is clear that KM06 and WG19 have the lowest percentage overlaps with all the other lists, with their highest overlap percentages being each other. This is due to their higher threshold values, which reduce the amount of storms the lists identify.

By comparing the overlaps between WG19 and WG19-50, we can see that lowering the SYM-H threshold required to identify a storm from −50 to −80 nT reduces the number of storms found by roughly 62%. We can repeat this with the overlaps between E11 and KM06, where E11 containing 100% of the storms that are also found in KM06, whereas KM06 contains only 33.4% of the storms in E11. The reduction in Dst threshold from −50 to −100 nT has reduced the number of storms identified by roughly 66%.

We can also see that although all the storms in WG19-0 are also in WG19, only 90.3% of the storms in WG19 are also in WG19-0. This is likely due to the length of the storms becoming longer due to the end point of the recovery phase being defined as when SYM-H reaches the quiet level.

5. Discussion

We analyzed the physical properties of the storms in each list by looking at the probability distributions of SYM-H both during and outside of geomagnetic storms. We found that the double peaked shape of the distributions for the WG19 lists with −15 nT SYM-H threshold were significantly different to the shape of the other lists. SYM-H can be used as a proxy for ring current energy (Sandhu et al., 2021), so the difference in SYM-H distributions between storm lists implies that the ring current energy distribution varies significantly between storm lists.

We defined the background distribution as the distribution of all the SYM-H data between the start of the first storm in the list and the end of the last storm and compared it with the distribution of the storms in the list. This

allowed us to see how different the geomagnetic storm SYM-H distribution was to the distribution of all time. We would expect the storm distribution to be skewed to more negative values than the background, as they are times of extreme geomagnetic activity. We found that all of the distributions were more negative than the background distributions, however the M18 and Tu15 distributions are surprisingly similar to the background. This implies that these lists do not identify conditions as extreme as the other lists. This could have impacts on forecasting if the lists that are used to train models do not identify the most extreme conditions, as these are the events which can cause the most disruption (Kappernman & Albertson, 1990; Pirjola, 2000; Smith et al., 2022). This is a known issue in machine learning called Class Imbalance, and has been discussed in the context of geomagnetic storms previously (e.g., Smith et al., 2024).

We then found the probability distribution of the three storm phases of the WG19 storms and found that the double peaked structure was due to the superposition of the distributions of the three storm phases, which were explicitly defined in the algorithm used to generate the WG19 lists. By comparison with the distributions of the WG19 (0 nT) variant, we showed that the position of the trough was directly connected to the definition of the quiet time SYM-H value used to define the storms, as this was used to identify the start and end of the storms. This means that the main and the recovery phases cannot have SYM-H values greater than the quiet time value, which causes a dip in the probability density at the bin containing the quiet time value. The fact that changing a single value in the algorithm could have such a large impact on the physical properties of the storms in the resulting list shows that the choice of storm definition can have a significant effect on the results that are drawn, and we intend to quantify this in other data sets in future work. The initial phase has a significantly different distribution to the main and the recovery phase, which is likely due to main phase being when the ring current strength increases, and the recovery phase when the ring current strength decreases (Akasofu & Chapman, 1961; Gonzalez et al., 1994), whereas the initial phase can contain a decrease in ring current strength as well as an increase (Gonzalez et al., 1999; Perreault & Akasofu, 1978). We also find that the overall distributions of all the lists are superpositions of the pre- and post-epoch distributions, which suggests that there are physical differences between the storm phases that could be used to create more robust definitions, and that these differences persist across the different geomagnetic storm identification methods.

The M18 list, which was the only other list to specify the start and end times of storms, used solar wind parameters and magnetic measurements to identify the start and end of the storms, which meant that the start and ends were less strictly constrained in SYM-H than storms in WG19.

The storm lists that were created using Dst data, KM06 and E11, have similarly shaped distributions, but KM06 has a wider and flatter distribution than E11. This is due to the KM06 Dst threshold value of −100 nT, compared to the E11 threshold value of −50 nT. This causes the KM06 list to be skewed to more extreme events than E11, and the rest of the storm lists, as KM06 has the most negative Dst or SYM-H threshold value required to identify a geomagnetic storm.

By comparing the Wasserstein distances between pairs of lists, we found that KM06 was the most different to the other lists, being the most similar to WG19. These two lists have similar SYM-H thresholds of −100 and −80 nT. We also see the effect of changing the threshold value by comparing the distances for the WG19 and WG19-50 lists. WG19 is more different than WG19-50 for every list other than KM06, which shows that the choice of SYM-H threshold used to define a geomagnetic storm can affect the list in a way that may be significant, as the only difference between the definitions used to generate WG19 and WG19-50 is the threshold value.

We defined the quiet time to be the time between the end of a storm and the start of the next storm for each storm list, and also compared these distributions to the background distribution. We found that for most of the storm lists, the quiet time distribution favored more positive SYM-H values than the background, which would be expected because the quiet distribution is the background distribution with the geomagnetic storms removed. The KM06 quiet distribution was almost the same as the background distribution, which is unexpected but likely due to the low number of storms in the list.

We also found that the quiet time distribution of Thomas et al. (2016) was similar to the other storm lists, despite the methodology including a step where extreme storms with minima below −200 nT were removed. In the time period covered by the original storm list only eight of these extreme storms were found, so the consequences of removing them from the storm list were minor. However, if a longer time period was considered using the same

methodology, the likelihood of finding extreme geomagnetic storms would increase. This would result in a greater discrepancy between "quiet time" as defined using the storm list and a true definition of quiet time.

We employed an SEA technique to compare the median behavior of the storms in each of the lists within a time range of 1 day before the time of minimum SYM-H and 3 days afterward. The overall behavior of the storms is consistent over all the lists that we have considered—there is a clear and sharp decrease in SYM-H at the epoch, and a gradual increase back to quiescence afterward. This shows that each of the lists identifies geomagnetic storms that have a common overall behavior that is not significantly impacted by changes in storm definition, however there are still some small differences. The steepness of the SYM-H decrease is influenced by the threshold value, as this sets the maximum value at the epoch, and the rate at which the SYM-H returns to the ambient level also differs between lists. In Figure 1 we can see that the temporal extent of storms in each list can vary significantly, however, due to our choice of time period these differences are not clear. By comparing our findings with those from the probability distributions, we can see that a SEA does not highlight the differences between the storm lists as well as the other methods we have considered.

By comparing the Dst and SYM-H SEAs for the KM06 and E11 lists, we showed that while the overall behavior of the storms is very similar in both indices, the SYM-H data includes finer detail than the Dst data. This is consistent with the findings of previous papers (Hutchinson et al., 2011; Wanliss & Showalter, 2006). SYM-H and Dst are commonly assumed to be approximately equal, as they both give indications of the behavior of the ring current, and have been used interchangeably (Brenner et al., 2021; Fok et al., 2011; Ohtani et al., 2001; Zhang et al., 2007). Most notably for this work, the M18 storm list was generated by using a threshold value defined using SYM-H, but gave the time of minimum Dst for each storm. Our findings have shown that Dst and SYM-H may not always be interchangeable when using them for measurements of extreme conditions, as well as the fact that Dst has hourly resolution so will not be sensitive to processes which occur on shorter timescales (Bergin et al., 2023; Katus & Liemohn, 2013; Sandhu et al., 2021). It has been previously found that Dst is unable to identify all storms, including long SIR driven storms (Borovsky & Shprits, 2017), and that there is a difference of around 20% in the measured SYM-H and Dst value during a storm (Katus & Liemohn, 2013).

From the temporal behavior of the storms shown in the superposed epoch analyses it can be seen that the E11 list is very similar to the two WG19 lists. However, when comparing probability distributions, the E11 list appears to be much more similar to the M18 list. This suggests that, when studying the behaviors and properties of geomagnetic storms, several methods of comparison should be used and the results compared, as certain storm lists can appear to be very different from each when compared using one method, but appear very similar when using another.

The time period covered by each storm list should also be taken into consideration when selecting a storm list, as the solar cycle can have significant impacts on the types of storms that occur, for example, CMEs are more likely to occur at solar maximum, whereas SIR occurrence peaks during the declining phase (Borovsky & Denton, 2006), and this could have impacts on the physical properties of the geomagnetic storms.

We calculated the percentage overlaps of each pair of storm lists and found that changes in the minimum SYM-H or Dst threshold for storm identification had a significant impact on the number of storms that are found in the same time period. By changing the threshold from −80 to −50 nT (WG19 and WG19-50) we found that the number of storms identified storms decreases by approximately 62%, and a change from −50 to −100 nT (E11 and KM06) leads to a 66% decrease.

6. Conclusions

Storm lists are typically used to study periods of extreme geomagnetic activity. Many studies that have included the use of a storm list have chosen to use only one list, often without discussion of any possible effects of this choice. We show that the choice of storm list can have significant effects on the lengths and probability distributions of the storms that are included in an investigation, and suggest that the consequences of a choice of storm list should be considered.

Using probability distributions we find that the way in which the start and the end of geomagnetic storms is defined can have a large impact on the physical properties of the storms that they identify. By imposing a strict quiet time SYM-H cutoff to be the end of the storms, the distribution of the WG19 lists shows a double peaked structure that is not seen for the other lists. We find that this structure is due to a superposition of the distributions

Table 2
Recommended Uses and Use Cases That Should Be Avoided for Each List

Storm list	Recommended uses	Use cases to avoid (*and reason*)
Kataoka and Miyoshi (2006)	• Study of extreme storms • Studies involving storm drivers	• General study of all types of storm (*Uses a threshold of* −100 nT) • Study of phenomena during storms (*States the time of maximum magnetic disturbance only*) • Studies where this is the only list used (*Significantly different to other storm lists*) • Studies that require high time resolution (*Created using Dst data*)
Echer et al. (2011)	• Study of storms over a long period of time • Comparisons between solar cycles	• Studies that require the exact storm identification process (*Storms were identified visually*) • Studies of phenomena during storms (*States the time of maximum magnetic disturbance only*) • Studies that require high time resolution (*Created using Dst data*)
Turner et al. (2015)	• No specific recommendations	• Studies that require at least a solar cycle worth of data (*Covers 3 years*) • Studies of phenomena during storms (*States the time of maximum magnetic disturbance only*)
Thomas et al. (2016)	• Studies that focus on the main phase	• Studies of extreme storms (*Excludes storms with minimum SYM-H* ≤ −200 nT) • Studies that include the initial and/or recovery phase (*Gives time of main phase onset and maximum magnetic disturbance*)
Murphy et al. (2018)	• Studies of phenomena during/outside storm times • Study of storms over a long period of time • Comparisons between solar cycles	• Studies that require a predefined SYM-H or Dst threshold (*Extended lists identifies storms using magnetic field behaviors*) • Studies that require high time resolution (*Defines the time of maximum magnetic disturbance using Dst data*)
Gabrielse et al. (2019)	• Studies that focus on the main and/or recovery phase • Studies that involve the storm driver	• Studies involving the initial phase (*States the time of main phase onset, maximum magnetic disturbance, and the end of recovery phase*) • Studies that require at least a solar cycle worth of data (*Covers 8 years*)
Walach and Grocott (2019)	• Studies that require storm definitions to be easily altered • Studies of phenomena during/outside storm times • Study of storms over a long period of time • Comparisons between solar cycles • Study of specific storm phases	• Studies of storm driver, unless used in conjunction with a catalog of drivers (*Uses magnetic indices to identify storms*)
Hua et al. (2022)	• No specific recommendations	• Studies of phenomena during storms (*States time of maximum magnetic disturbance only*) • Studies that require at least a solar cycle worth of data (*Covers 5 years*)

of the three storm phases, with the initial phase having a significantly different shape to the main and recovery phases. We also show that the SYM-H distribution of storms in lists that do not define the times of the different phases are also superpositions of multiple distributions, and that the pre- and post-epoch SYM-H distributions are physically distinct in all lists.

Finally we show that the overall temporal behavior of geomagnetic storms in a time period from one day before the epoch to 3 days after is largely the same across storm lists, and is not significantly affected by the choice of either Dst or SYM-H, except for the loss of fine detail due to the lower resolution of Dst data.

We also find that the minimum threshold value of SYM-H or Dst has a significant impact on the number of storms that are identified over the same time period, with a change in threshold from −50 to −80 nT resulting in a decrease in the number of storms identified by approximately 62%. This is of interest as the threshold value is a significant parameter in storm lists that identify geomagnetic storms in this manner.

7. Recommendations

Based on our findings, we have made some suggestions on how to choose a storm list. These recommendations will not be able to cover all possible use cases, so it is possible that modifications will be required for a specific case-study. Table 2 shows the types of studies that each storm list is best suited for, as well as types of studies where certain lists should be avoided, and we explain these recommendations in detail below.

Firstly, Walach and Grocott (2019) specifies strict start and end points for each of the storm phases, which is not available from the other lists, and this allows for more in-depth research of specific parts of a geomagnetic storm. The algorithm can also be easily applied to any time period where SYM-H data is available (Coxon & Walach, 2025), and the parameters for identifying a storm can be adjusted to generate lists with different properties. When the SYM-H threshold is changed from −80 to −50 nT, the resulting list is in agreement with the other storm lists that use a threshold of −50 nT. The WG19 algorithm could therefore be used to extend the shorter −50 nT lists to longer time periods, as well as better constraining the start and end of the storms. Overall, WG19 is a list that would be well suited for most applications, and the algorithm can be altered for specific case studies.

The period of the solar cycle that a storm list covers should be taken into account when choosing either a pre-made storm list or a definition to apply to a different data set. The occurrence rates of CMEs and SIRs, the main drivers of geomagnetic storms, vary throughout the solar cycle, and a list that only covers a short time period may be biased toward one solar wind driver over the other. It is also known that CMEs produce a larger perturbation in the magnetic field than SIRs (Denton et al., 2006), so more extreme storms are more likely to be driven by CMEs than by SIRs. Therefore, both the portion of the solar cycle that a storm list covers and the threshold value required to identify a storm should be taken into account as these may introduce biases with regards to the drivers of the storms. We will investigate the impacts of storm drivers on the properties of the storms in a future paper. The lists that cover entire solar cycles (or multiple cycles) and are less likely to be biased are WG19, M18, Th16, and E11.

We have considered two storm lists that explicitly state the driver responsible for each storm, Kataoka and Miyoshi (2006) and Gabrielse et al. (2019), however KM06 is significantly different from the other lists in both probability distribution and SEA, and caution should be taken if this list is to be used. G19 states if a storm is due to a CME, HSS, or other, and is not significantly different to the other lists, but covers only 2008 to 2016. We suggest that if the drivers of geomagnetic storms is an area of interest for a time period outside of the range covered by G19, CME and SIR catalogs, such as the SOHO LASCO CME catalog (http://cdaw.gsfc.nasa.gov/CME_list), the STEREO ICME and SIR catalogs (https://stereo-dev.epss.ucla.edu/l3_events), and the list by Chi et al. (2018), should be used alongside another storm list.

Another reason to carefully consider the time period covered by a storm list is the particular solar cycle that is covered by the list. If the research topic is not constrained to a specific solar cycle, we recommend use of a storm list that covers multiple solar cycles, such as WG19. M18 also covers multiple solar cycles, however it contains storms where the end time is cited to be prior to the start time, and care should be taken to check the validity of the storms. If a shorter time period is required, the different strengths of each cycle should be taken into account, for example, the difference between cycle 22 and cycle 24.

Due to the fact that a list of storm times also implicitly defines a list of non-storm times, storm lists may be used when studying the magnetosphere outside of geomagnetic storms. In such cases, care must be taken to avoid storm lists such as Thomas et al. (2016) where extreme or complex storms are not included in the final list. We suggest use of a list that does not remove extreme storms and that explicitly states the start and end times of each storm, such as WG19 or M18.

Finally, we suggest that multiple storm lists should be considered and compared using at least two methods in order to identify any biases that may be introduced. A method of comparing the temporal behaviors, such as a SEA, and a method of comparing the physical properties of the storms, such as a probability distribution, should be considered prior to the selection of a storm list so that the effects of the storm identification criteria can be properly understood.

Inclusion in Global Research Statement

As applicable.

Conflict of Interest

The authors declare no conflicts of interest relevant to this study.

Availability Statement

The OMNI SYM-H data used in the study was downloaded from Coordinated Data Analysis Web, NASA via https://cdaweb.gsfc.nasa.gov/ (King & Papitashvili, 2020). Dst data was used to study storm lists that were generated using Dst data and was downloaded from WDC for Geomagnetism, Kyoto via https://wdc.kugi.kyoto-u.ac.jp/dstdir/ (Sugiura & Kamei, 1991). OMNI CDF files were read in Python using cdflib version 1.2.3 (Stansby et al., 2022). Data Analysis was carried out using NumPy version 2.3.4 (Harris et al., 2020). Kernel Density Estimation was applied to the SYM-H distributions for comparison with histograms using Scikit-learn version 1.5.0 (Pedregosa et al., 2011) Figures 2–9 (and all figures in Supporting Information S1) were created using Matplotlib version 3.10.6, via https://doi.org/10.5281/zenodo.16999430, available under the Matplotlib license at https://matplotlib.org/ (Hunter, 2007). The software used to generate the alternate versions of Walach and Grocott (2019) is preserved at https://github.com/johncoxon/storm-lists (Coxon & Walach, 2025). The software used for data analysis and generation of Figures 2–9 (and all figures in Supporting Information S1) is preserved at https://github.com/apatrick01/Storm-Lists (Patrick, 2025).

Acknowledgments
The authors acknowledge invaluable technical support provided by Alexander D. Tempest. We gratefully acknowledge the support from Northumbria University NU: Opportunities scheme that enabled Isobel Lockley's initial work in this area. John C. Coxon was supported by Science and Technology Facilities Council (STFC) Ernest Rutherford Fellowship ST/V004883/1. Sarah Bentley was supported by STFC Grant ST/X001008/1. Maria-Theresia Walach acknowledges funding from UKRI STFC through the Ernest Rutherford Fellowship ST/X003663/1. Kyle R Murphy is partially funded by CSA Grant 23SUSTDYNA. I. Jonathan Rae was supported by STFC Grant ST/X001008/1 and Natural Environment Research Council (NERC) Grant NE/W003198/1.

References

Akasofu, S., & Chapman, S. (1961). The ring current, geomagnetic disturbance, and the Van Allen radiation belts. *Journal of Geophysical Research*, *66*(5), 1321–1350. https://doi.org/10.1029/JZ066i005p01321

Babu, G. J., & Singh, K. (1983). Inference on means using the bootstrap. *Annals of Statistics*, *11*(3), 999–1003. https://doi.org/10.1214/aos/1176346267

Balan, N., Tulasiram, S., Kamide, Y., Batista, I. S., Souza, J. R., Shiokawa, K., et al. (2017). Automatic selection of Dst storms and their seasonal variations in two versions of Dst in 50 years. *Earth Planets and Space*, *69*(1), 59. https://doi.org/10.1186/s40623-017-0642-2

Bergin, A., Chapman, S. C., & Gjerloev, J. W. (2020). AE, D_{ST}, and their SuperMAG counterparts: The effect of improved spatial resolution in geomagnetic indices. *Journal of Geophysical Research: Space Physics*, *125*(5), e2020JA027828. https://doi.org/10.1029/2020JA027828

Bergin, A., Chapman, S. C., Watkins, N. W., Moloney, N. R., & Gjerloev, J. W. (2023). Extreme event statistics in Dst, SYM-H, and SMR geomagnetic indices. *Space Weather*, *21*(3), e2022SW003304. https://doi.org/10.1029/2022SW003304

Borovsky, J. E., & Denton, M. H. (2006). Differences between CME-driven storms and CIR-driven storms. *Journal of Geophysical Research*, *111*(A7). https://doi.org/10.1029/2005JA011447

Borovsky, J. E., & Shprits, Y. Y. (2017). Is the Dst index sufficient to define all geospace storms? *Journal of Geophysical Research: Space Physics*, *122*(11), 11543–11547. https://doi.org/10.1002/2017JA024679

Bower, G. E., Milan, S. E., Imber, S., Schillings, A., Fleetham, A., Beggan, C., & Gjerloev, J. W. (2025). Asymmetry in the ring current during geomagnetic disturbances. *Journal of Geophysical Research: Space Physics*, *130*(3), e2024JA033492. https://doi.org/10.1029/2024JA033492

Brenner, A., Pulkkinen, T. I., Al Shidi, Q., & Toth, G. (2021). Stormtime energetics: Energy transport across the magnetopause in a global MHD simulation. *Frontiers in Astronomy and Space Sciences*, *8*, 756732. https://doi.org/10.3389/fspas.2021.756732

Campbell, W. H. (2004). Failure of Dst index fields to represent a ring current. *Space Weather*, *2*(8). https://doi.org/10.1029/2003SW000041

Chi, Y., Shen, C., Luo, B., Wang, Y., & Xu, M. (2018). Geoeffectiveness of stream interaction regions from 1995 to 2016. *Space Weather*, *16*(12), 1960–1971. https://doi.org/10.1029/2018SW001894

Collado-Villaverde, A., Muñoz, P., & Cid, C. (2024). Classifying and bounding geomagnetic storms based on the SYM-H and ASY-H indices. *Natural Hazards*, *120*(2), 1141–1162. https://doi.org/10.1007/s11069-023-06241-1

Cowley, S. W. H. (Ed.) (1981). Magnetospheric and ionospheric flow and the interplanetary magnetic field. In *AGARD Conference Proceedings No. 295, The Physical Basis of the Ionosphere in the Solar-Terrestrial System*. NATO Science and Technology Organization.

Cowley, S. W. H., & Lockwood, M. (1992). Excitation and decay of solar wind-driven flows in the magnetosphere-ionosphere system. *Annales Geophysicae*, *10*(1–2), 103–115.

Coxon, J. C., Chisham, G., Freeman, M. P., Forsyth, C., Walach, M.-T., Murphy, K. R., et al. (2023). Extreme Birkeland currents are more likely during geomagnetic storms on the dayside of the Earth. *Journal of Geophysical Research: Space Physics*, *128*(12), e2023JA031946. https://doi.org/10.1029/2023JA031946

Coxon, J. C., & Walach, M.-T. (2025). Storm-lists. *Zenodo*. https://doi.org/10.5281/zenodo.17525074

Cramer, W. D., Raeder, J., Toffoletto, F. R., Gilson, M., & Hu, B. (2017). Plasma sheet injections into the inner magnetosphere: Two-way coupled OpenGGCM-RCM model results. *Journal of Geophysical Research: Space Physics*, *122*(5), 5077–5091. https://doi.org/10.1002/2017JA024104

Daglis, I. A. (2006). Ring current dynamics. *Space Science Reviews*, *124*(1), 183–202. https://doi.org/10.1007/s11214-006-9104-z

Daglis, I. A., Thorne, R. M., Baumjohann, W., & Orsini, S. (1999). The terrestrial ring current: Origin, formation, and decay. *Reviews of Geophysics*, *37*(4), 407–438. https://doi.org/10.1029/1999RG900009

Denton, M. H., Borovsky, J. E., Skoug, R. M., Thomsen, M. F., Lavraud, B., Henderson, M. G., et al. (2006). Geomagnetic storms driven by ICME- and CIR-dominated solar wind. *Journal of Geophysical Research*, *111*(A7). https://doi.org/10.1029/2005JA011436

Dessler, A. J., & Parker, E. N. (1959). Hydromagnetic theory of geomagnetic storms. *Journal of Geophysical Research*, *64*(12), 2239–2252. https://doi.org/10.1029/JZ064i012p02239

Dungey, J. W. (1961). Interplanetary magnetic field and the auroral zones. *Physical Review Letters*, *6*(2), 47–48. https://doi.org/10.1103/PhysRevLett.6.47

Echer, E., Gonzalez, W., & Tsurutani, B. (2011). Statistical studies of geomagnetic storms with peak Dst ≤ 50 nt from 1957 to 2008. *Journal of Atmospheric and Solar-Terrestrial Physics*, *73*(11), 1454–1459. https://doi.org/10.1016/j.jastp.2011.04.021

Eggington, J. W. B., Desai, R. T., Mejnertsen, L., Chittenden, J. P., & Eastwood, J. P. (2022). Time-varying magnetopause reconnection during sudden commencement: Global MHD simulations. *Journal of Geophysical Research: Space Physics*, *127*(4), e2021JA030006. https://doi.org/10.1029/2021JA030006

Fok, M.-C., Moore, T. E., Slinker, S. P., Fedder, J. A., Delcourt, D. C., Nosé, M., & Chen, S.-H. (2011). Modeling the superstorm in November 2003. *Journal of Geophysical Research*, *116*(A1). https://doi.org/10.1029/2010JA015720

Forsyth, C., Watt, C. E. J., Rae, I. J., Fazakerley, A. N., Kalmoni, N. M. E., Freeman, M. P., et al. (2014). Increases in plasma sheet temperature with solar wind driving during substorm growth phases. *Geophysical Research Letters*, *41*(24), 8713–8721. https://doi.org/10.1002/2014GL062400

Fu, S., & Sun, W. (2026). Planetary magnetospheric convection models: The Dungey cycle and the Vasyliūnas cycle. *Science China Earth Sciences*, *69*(3), 1167–1176. https://doi.org/10.1007/s11430-025-1865-6

Gabrielse, C., Pinto, V., Nishimura, Y., Lyons, L., Gallardo-Lacourt, B., & Deng, Y. (2019). Storm time mesoscale plasma flows in the nightside high-latitude ionosphere: A statistical survey of characteristics. *Geophysical Research Letters*, *46*(8), 4079–4088. https://doi.org/10.1029/2018GL081539

Gonzalez, W. D., Joselyn, J. A., Kamide, Y., Kroehl, H. W., Rostoker, G., Tsurutani, B. T., & Vasyliunas, V. M. (1994). What is a geomagnetic storm? *Journal of Geophysical Research*, *99*(A4), 5771–5792. https://doi.org/10.1029/93JA02867

Gonzalez, W. D., Tsurutani, B. T., & Clúa de Gonzalez, A. L. (1999). Interplanetary origin of geomagnetic storms. *Space Science Reviews*, *88*(3), 529–562. https://doi.org/10.1023/A:1005160129098

Harris, C. R., Millman, K. J., van der Walt, S. J., Gommers, R., Virtanen, P., Cournapeau, D., et al. (2020). Array programming with NumPy. *Nature*, *585*(7825), 357–362. https://doi.org/10.1038/s41586-020-2649-2

Hua, M., Bortnik, J., & Ma, Q. (2022). Upper limit of outer radiation belt electron acceleration driven by whistler-mode chorus waves. *Geophysical Research Letters*, *49*(15), e2022GL099618. https://doi.org/10.1029/2022GL099618

Hunter, J. D. (2007). Matplotlib: A 2D graphics environment. *Computing in Science & Engineering*, *9*(3), 90–95. https://doi.org/10.1109/MCSE.2007.55

Hutchinson, J. A., Wright, D. M., & Milan, S. E. (2011). Geomagnetic storms over the last solar cycle: A superposed epoch analysis. *Journal of Geophysical Research*, *116*(A9). https://doi.org/10.1029/2011JA016463

Iyemori, T. (1990). Storm-time magnetospheric currents inferred from mid-latitude geomagnetic field variations. *Journal of Geomagnetism and Geoelectricity*, *42*(11), 1249–1265. https://doi.org/10.5636/jgg.42.1249

Joselyn, J. A., & Tsurutani, B. T. (1990). Geomagnetic sudden impulses and storm sudden commencements: A note on terminology. *EOS Transactions of the American Geophysical Union*, *71*(47), 1808–1809. https://doi.org/10.1029/90EO00350

Kantorovich, L. V. (1960). Mathematical methods of organizing and planning production. *Management Science*, *6*(4), 366–422. https://doi.org/10.1287/mnsc.6.4.366

Kappenman, J., & Albertson, V. (1990). Bracing for the geomagnetic storms. *IEEE Spectrum*, *27*(3), 27–33. https://doi.org/10.1109/6.48847

Kataoka, R., & Miyoshi, Y. (2006). Flux enhancement of radiation belt electrons during geomagnetic storms driven by coronal mass ejections and corotating interaction regions. *Space Weather*, *4*(9). https://doi.org/10.1029/2005SW000211

Katus, R. M., & Liemohn, M. W. (2013). Similarities and differences in low- to middle-latitude geomagnetic indices. *Journal of Geophysical Research: Space Physics*, *118*(8), 5149–5156. https://doi.org/10.1002/jgra.50501

Killey, S., Rae, I. J., Smith, A. W., Bentley, S. N., Watt, C. E. J., Chakraborty, S., et al. (2025). Identifying typical relativistic electron pitch angle distributions: Evolution during geomagnetic storms. *Geophysical Research Letters*, *52*(3), e2024GL112900. https://doi.org/10.1029/2024GL112900

King, J. H., & Papitashvili, N. E. (2020). Omni 1-min data set. *NASA Space Physics Data Facility*. https://doi.org/10.48322/45BB-8792

Kivelson, M. G., & Russell, C. T. (1995). *Introduction to space physics*. Cambridge University Press.

Kumar, S., Garg, S., Takur, P. S., Soni, S. L., & Tripathi, O. P. (2026). Investigating the interplanetary causes of severe geomagnetic storms during solar cycle 23 using SYM-H and OMNI data. *Rendiconti Lincei. Scienze Fisiche e Naturali*, *37*(1), 139–153. https://doi.org/10.1007/s12210-025-01390-w

Loewe, C. A., & Prölss, G. W. (1997). Classification and mean behavior of magnetic storms. *Journal of Geophysical Research*, *102*(A7), 14209–14213. https://doi.org/10.1029/96JA04020

Love, J. J., Rigler, E. J., Pulkkinen, A., & Riley, P. (2015). On the lognormality of historical magnetic storm intensity statistics: Implications for extreme-event probabilities. *Geophysical Research Letters*, *42*(16), 6544–6553. https://doi.org/10.1002/2015GL064842

Manu, V., Balan, N., Zhang, Q.-H., & Xing, Z.-Y. (2023). Double superposed epoch analysis of geomagnetic storms and corresponding solar wind and IMF in solar cycles 23 and 24. *Space Weather*, *21*(3), e2022SW003314. https://doi.org/10.1029/2022SW003314

Milan, S. E., Carter, J. A., Bower, G. E., Imber, S. M., Paxton, L. J., Anderson, B. J., et al. (2020). Dual-lobe reconnection and horse-collar auroras. *Journal of Geophysical Research: Space Physics*, *125*(10), e2020JA028567. https://doi.org/10.1029/2020JA028567

Murphy, K. R., Watt, C. E. J., Mann, I. R., Jonathan Rae, I., Sibeck, D. G., Boyd, A. J., et al. (2018). The global statistical response of the outer radiation belt during geomagnetic storms. *Geophysical Research Letters*, *45*(9), 3783–3792. https://doi.org/10.1002/2017GL076674

Ohtani, S., Nosé, M., Rostoker, G., Singer, H., Lui, A. T. Y., & Nakamura, M. (2001). Storm-substorm relationship: Contribution of the tail current to Dst. *Journal of Geophysical Research*, *106*(A10), 21199–21209. https://doi.org/10.1029/2000JA000400

Parker, E. N. (1962). Dynamics of the geomagnetic storm. *Space Science Reviews*, *1*(1), 62–99. https://doi.org/10.1007/BF00174636

Partamies, N., Juusola, L., Tanskanen, E., & Kauristie, K. (2013). Statistical properties of substorms during different storm and solar cycle phases. *Annales Geophysicae*, *31*(2), 349–358. https://doi.org/10.5194/angeo-31-349-2013

Patrick, A. M. (2025). apatrick01/storm-lists: v1.0.0. *Zenodo*. https://doi.org/10.5281/zenodo.17859199

Pedregosa, F., Varoquaux, G., Gramfort, A., Michel, V., Thirion, B., Grisel, O., et al. (2011). Scikit-learn: Machine learning in Python. *Journal of Machine Learning Research*, *12*, 2825–2830.

Perreault, P., & Akasofu, S. I. (1978). A study of geomagnetic storms. *Geophysical Journal International*, *54*(3), 547–573. https://doi.org/10.1111/j.1365-246X.1978.tb05494.x

Pirjola, R. (2000). Geomagnetically induced currents during magnetic storms. *IEEE Transactions on Plasma Science*, *28*(6), 1867–1873. https://doi.org/10.1109/27.902215

Reeves, G. D., McAdams, K. L., Friedel, R. H. W., & O'Brien, T. P. (2003). Acceleration and loss of relativistic electrons during geomagnetic storms. *Geophysical Research Letters*, *30*(10). https://doi.org/10.1029/2002GL016513

Samwel, S., & Miteva, R. (2023). Correlations between space weather parameters during intense geomagnetic storms: Analytical study. *Advances in Space Research*, *72*(8), 3440–3453. https://doi.org/10.1016/j.asr.2023.07.053

Sandhu, J. K., Rae, I. J., Freeman, M. P., Forsyth, C., Gkioulidou, M., Reeves, G. D., et al. (2018). Energization of the ring current by substorms. *Journal of Geophysical Research: Space Physics*, *123*(10), 8131–8148. https://doi.org/10.1029/2018JA025766

Sandhu, J. K., Rae, I. J., & Walach, M.-T. (2021). Challenging the use of ring current indices during geomagnetic storms. *Journal of Geophysical Research: Space Physics*, *126*(2), e2020JA028423. https://doi.org/10.1029/2020JA028423

Shue, J.-H., Song, P., Russell, C. T., Steinberg, J. T., Chao, J. K., Zastenker, G., et al. (1998). Magnetopause location under extreme solar wind conditions. *Journal of Geophysical Research*, *103*(A8), 17691–17700. https://doi.org/10.1029/98JA01103

Siscoe, G. L., & Huang, T. S. (1985). Polar cap inflation and deflation. *Journal of Geophysical Research*, *90*(A1), 543–547. https://doi.org/10.1029/JA090iA01p00543

Smith, A. W., Forsyth, C., Rae, I. J., Garton, T. M., Jackman, C. M., Bakrania, M., et al. (2022). On the considerations of using near real time data for space weather hazard forecasting. *Space Weather*, *20*(7), e2022SW003098. https://doi.org/10.1029/2022SW003098

Smith, A. W., Rae, I. J., Forsyth, C., Coxon, J. C., Walach, M.-T., Lao, C. J., et al. (2024). Space weather forecasts of ground level space weather in the UK: Evaluating performance and limitations. *Space Weather*, *22*(11), e2024SW003973. https://doi.org/10.1029/2024SW003973

Sonnerup, B. U. Ö., Paschmann, G., Papamastorakis, I., Sckopke, N., Haerendel, G., Bame, S. J., et al. (1981). Evidence for magnetic field reconnection at the earth's magnetopause. *Journal of Geophysical Research*, *86*(A12), 10049–10067. https://doi.org/10.1029/JA086iA12p10049

Stansby, D., Harter, B., SDC, M., scivision, van Kemenade, H., Burrell, A., et al. (2022). *Mavensdc/cdflib*. Zenodo. https://doi.org/10.5281/zenodo.1481144

Staples, F. A., Kellerman, A., Murphy, K. R., Rae, I. J., Sandhu, J. K., & Forsyth, C. (2022). Resolving magnetopause shadowing using multimission measurements of phase space density. *Journal of Geophysical Research: Space Physics*, *127*(2), e2021JA029298. https://doi.org/10.1029/2021JA029298

Sugiura, M., & Kamei, T. (1991). *IAGA Bulletin No 40 – Equatorial Dst index 1957–1986*. ISGI Publications Office.

Thomas, E. G., Baker, J. B. H., Ruohoniemi, J. M., Coster, A. J., & Zhang, S.-R. (2016). The geomagnetic storm time response of GPS total electron content in the North American sector. *Journal of Geophysical Research: Space Physics*, *121*(2), 1744–1759. https://doi.org/10.1002/2015JA022182

Trattner, K. J., Mulcock, J. S., Petrinec, S. M., & Fuselier, S. A. (2007). Location of the reconnection line at the magnetopause during southward IMF conditions. *Geophysical Research Letters*, *34*(3). https://doi.org/10.1029/2006GL028397

Trattner, K. J., Thresher, S., Trenchi, L., Fuselier, S. A., Petrinec, S. M., Peterson, W. K., & Marcucci, M. F. (2017). On the occurrence of magnetic reconnection equatorward of the cusps at the Earth's magnetopause during northward IMF conditions. *Journal of Geophysical Research: Space Physics*, *122*(1), 605–617. https://doi.org/10.1002/2016JA023398

Tsurutani, B. T., Gonzalez, W. D., Gonzalez, A. L. C., Guarnieri, F. L., Gopalswamy, N., Grande, M., et al. (2006). Corotating solar wind streams and recurrent geomagnetic activity: A review. *Journal of Geophysical Research*, *111*(A7). https://doi.org/10.1029/2005JA011273

Turner, D. L., O'Brien, T. P., Fennell, J. F., Claudepierre, S. G., Blake, J. B., Kilpua, E. K. J., & Hietala, H. (2015). The effects of geomagnetic storms on electrons in Earth's radiation belts. *Geophysical Research Letters*, *42*(21), 9176–9184. https://doi.org/10.1002/2015GL064747

Vaserstein, L. N. (1969). Markov processes over denumerable products of spaces, describing large systems of automata. *Problems of Information Transmission*, *5*, 64–72. Retrieved from https://www.mathnet.ru/rus/ppi/v5/i3/p64

Walach, M.-T., & Grocott, A. (2019). Superdarn observations during geomagnetic storms, geomagnetically active times, and enhanced solar wind driving. *Journal of Geophysical Research: Space Physics*, *124*(7), 5828–5847. https://doi.org/10.1029/2019JA026816

Walach, M.-T., Milan, S. E., Yeoman, T. K., Hubert, B. A., & Hairston, M. R. (2017). Testing nowcasts of the ionospheric convection from the expanding and contracting polar cap model. *Space Weather*, *15*(4), 623–636. https://doi.org/10.1002/2017SW001615

Wanliss, J. A., & Showalter, K. M. (2006). High-resolution global storm index: Dst versus SYM-H. *Journal of Geophysical Research*, *111*(A2). https://doi.org/10.1029/2005JA011034

Wharton, S. J., Rae, I. J., Sandhu, J. K., Walach, M.-T., Wright, D. M., & Yeoman, T. K. (2020). The changing eigenfrequency continuum during geomagnetic storms: Implications for plasma mass dynamics and ULF wave coupling. *Journal of Geophysical Research: Space Physics*, *125*(6), e2019JA027648. https://doi.org/10.1029/2019JA027648

Williams, D. J. (1985). Dynamics of the earth's ring current: Theory and observation. *Space Science Reviews*, *42*(3), 375–396. https://doi.org/10.1007/BF00214994

Yermolaev, Y. I., Nikolaeva, N. S., Lodkina, I. G., & Yermolaev, M. Y. (2010). Specific interplanetary conditions for CIR-, Sheath-, and ICME-induced geomagnetic storms obtained by double superposed epoch analysis. *Annales Geophysicae*, *28*(12), 2177–2186. https://doi.org/10.5194/angeo-28-2177-2010

Yokoyama, N., & Kamide, Y. (1997). Statistical nature of geomagnetic storms. *Journal of Geophysical Research*, *102*(A7), 14215–14222. https://doi.org/10.1029/97JA00903

Zhang, J., Liemohn, M. W., De Zeeuw, D. L., Borovsky, J. E., Ridley, A. J., Toth, G., et al. (2007). Understanding storm-time ring current development through data-model comparisons of a moderate storm. *Journal of Geophysical Research*, *112*(A4). https://doi.org/10.1029/2006JA011846

Zhang, J., Liemohn, M. W., Kozyra, J. U., Thomsen, M. F., Elliott, H. A., & Weygand, J. M. (2006). A statistical comparison of solar wind sources of moderate and intense geomagnetic storms at solar minimum and maximum. *Journal of Geophysical Research*, *111*(A1). https://doi.org/10.1029/2005JA011065